JACS
JOURNAL OF THE AMERICAN CHEMICAL SOCIETY

Article

pubs.acs.org/JACS

TEMPO Monolayers on Si(100) Electrodes: Electrostatic Effects by the Electrolyte and Semiconductor Space-Charge on the Electroactivity of a Persistent Radical

Long Zhang,[†] Yan Boris Vogel,[†] Benjamin B. Noble,[‡] Vinicius R. Gonçales,[§] Nadim Darwish,[∥] Anton Le Brun,[⊥] J. Justin Gooding,[§] Gordon G. Wallace,*[,†] Michelle L. Coote,*[,‡] and Simone Ciampi*[,†]

[†]ARC Centre of Excellence for Electromaterials Science, Intelligent Polymer Research Institute, University of Wollongong, Wollongong, New South Wales 2500, Australia

[‡]ARC Centre of Excellence for Electromaterials Science, Research School of Chemistry, Australian National University, Canberra, Australian Capital Territory 2601, Australia

[§]School of Chemistry, Australian Centre for NanoMedicine and ARC Centre of Excellence for Convergent Bio-Nano Science and Technology, The University of New South Wales, Sydney, New South Wales 2052, Australia

[∥]Institut de Bioenginyeria de Catalunya (IBEC), Baldiri Reixac 15-21, Barcelona 08028, Catalonia Spain

[⊥]Bragg Institute, Australian Nuclear Science and Technology Organisation (ANSTO), Locked Bag 2001, Kirrawee DC, New South Wales 2232, Australia

Supporting Information

ABSTRACT: This work demonstrates the effect of electrostatic interactions on the electroactivity of a persistent organic free radical. This was achieved by chemisorption of molecules of 4-azido-2,2,6,6-tetramethyl-1-piperdinyloxy (4-azido-TEMPO) onto monolayer-modified Si(100) electrodes using a two-step chemical procedure to preserve the open-shell state and hence the electroactivity of the nitroxide radical. Kinetic and thermodynamic parameters for the surface electrochemical reaction are investigated experimentally and analyzed with the aid of electrochemical digital simulations and quantum-chemical calculations of a theoretical model of the tethered TEMPO system. Interactions between the electrolyte anions and the TEMPO grafted on highly doped, i.e., metallic, electrodes can be tuned to predictably manipulate the oxidizing power of surface nitroxide/oxoammonium redox couple, hence showing the practical importance of the electrostatics on the electrolyte side of the radical monolayer. Conversely, for monolayers prepared on the poorly doped electrodes, the electrostatic interactions between the tethered TEMPO units and the semiconductor-side, i.e., space-charge, become dominant and result in drastic kinetic changes to the electroactivity of the radical monolayer as well as electrochemical nonidealities that can be explained as an increase in the self-interaction "*a*" parameter that leads to the Frumkin isotherm.

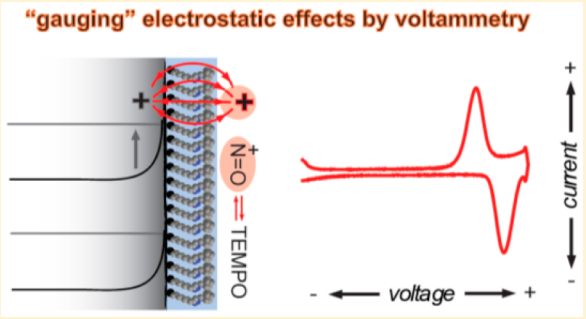

1. INTRODUCTION

To realize the full technological potential that molecular and supramolecular systems hold, our ability to control molecular topology, and hence function, needs to be coupled to the sturdiness of a solid device.[1] Persistent organic free radicals have a key role in chemistry and biology,[2] and nitroxide radicals, such as the 2,2,6,6-tetramethyl-1-piperidinyloxyl radical generally referred to as TEMPO, and its derivatives are very interesting both from a fundamental[3] as well as from an applied[4] point of view. Assembly of persistent radicals on solid surfaces by physisorption is often complicated by the competition between the thermodynamic assembly and unwanted kinetic traps;[5] hence, chemical routes to tether TEMPO species onto a solid, such as gold- and carbon-based materials are starting to appear.[6] Silicon, in particular the (100) orientation, remains the technologically most relevant material of our age,[7] and this material is still bringing fresh momentum to the fields of electrochemistry,[8] spintronics,[9] and molecular electronics.[10] No reports are available for the tethering of nitroxide radicals on silicon electrodes. This is presumably because of the ease of binding between silicon surface bonds and the unpaired valence electron of the singly occupied molecular orbital of the TEMPO molecule, which would result in the loss of the free radical character.[11] Here we address this issue using a two-step chemical route to preserve the unpaired spin upon grafting. A Si(100)−H surface is first functionalized by the thermal hydrosilylation of α,ω-alkynes to yield a short

Received: May 9, 2016
Published: July 4, 2016

DOI: 10.1021/jacs.6b04788
J. Am. Chem. Soc. 2016, 138, 9611−9619

functional monolayer where direct electrical communication between a grafted molecule and the substrate is still possible.[12] Thereafter, TEMPO is attached with the radical preserved.

The properties of a near-surface region are remarkably different to the properties of the bulk. For instance, issues of mass transport can be neglected. Similarly, the chemical interactions of a grafted molecule with either the solid, neighboring molecules or supporting electrolyte molecules may dramatically change the chemical,[13] optical,[14] or redox[15] properties. The purpose of the current study is to investigate how the electrostatic interactions between surface-grafted TEMPO units and residual charges in the semiconductor space-charge, or electrolyte ions, can predictably tune the electroactivity of a common radical species. To achieve both the passivation of the substrate against anodic decomposition[12a] as well as to circumvent the high reactivity of the Si−H surface toward the oxygen function in the TEMPO molecule, we have relied on an established wet chemistry protocol to prepare alkyne-terminated monolayers (**S-1**, Scheme 1).[12b,16] The

Scheme 1. Thermal Hydrosilylation of 1,8-Nonadiyne 1 at a Si(100)-H Electrode (S-1) and Covalent Attachment of 4-Azido-TEMPO 2 via CuAAC "Click" Reactions to Yield the Redox-Active Radical Film (S-2)

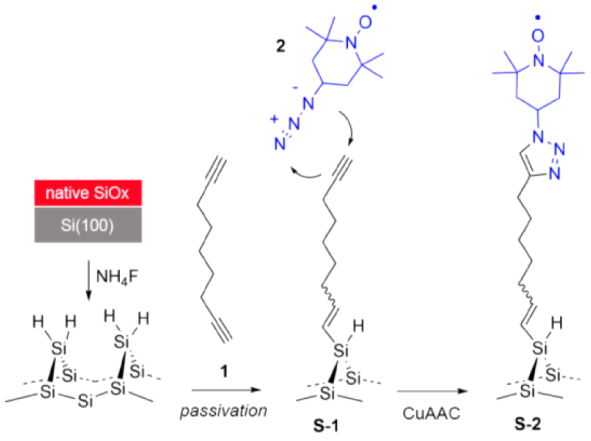

chemical passivation of the Si(100) surface, as depicted in Scheme 1, is generally proven to be a difficult experimental task,[17] and a definitive mechanism for the thermal hydrosilylation of 1-alkynes is still debated.[18] The mainly dihydride phase (=SiH_2) of the chemically etched (100) surface[19] does not allow for a complete reaction of Si−H sites,[20] but if the monolayer can retain a degree of $\pi-\pi$ interactions, then anodic decomposition of the substrate can be greatly limited.[12a] The 1-alkyne moiety that remains exposed at the monolayer distal end in **S-1** samples can engage in highly selective copper-catalyzed alkyne−azide cycloaddition reactions (CuAAC[21]) to immobilize an azide-tagged version of TEMPO (**S-2**). This chemistry opens up access to an interface where (i) the Si/C contrast enables one to complement analytical electrochemical methods with surface-sensitive X-ray spectroscopic techniques[12a] and (ii) the presence of a band gap in the semiconducting substrate allows one to shift redox reactions contra-thermodynamically if assisted by visible radiation, i.e., energetic gain in a catalytic application of the radical film.

2. EXPERIMENTAL METHODS

2.1. Chemicals and Materials. Unless otherwise noted, all chemicals were of analytical grade and used as received. Chemicals used in surface modification procedures and electrochemical experiments were of high purity (>99%). Hydrogen peroxide (30 wt % in water), ammonium fluoride (PuranalTM, 40 wt % in water), and sulfuric acid (PuranalTM, 95−97%) used in wafer cleaning and etching procedures were of semiconductor grade from Sigma-Aldrich. 1,8-Nonadiyne (**1**, Sigma-Aldrich, 98%) was redistilled from sodium borohydride (Sigma-Aldrich, 99+%) under reduced pressure (80 °C, 10−12 Torr) and stored under high-purity argon atmosphere prior to use. 4-Azido-2,2,6,6-tetramethyl-1-piperdinyloxy (**2**, 4-azido-TEMPO) was prepared in two steps from 4-hydroxy-2,2,6,6-tetramethyl-1-piperdinyloxy (4-hydroxy-TEMPO, Sigma-Aldrich, 97%) through published methods[22] with minor modifications (Supporting Information). Thin-layer chromatography (TLC) was performed on silica gel using Merck aluminum sheets (60 F_{254}). Merck 60 Å silica gel (220−400 mesh particle size) was used for column chromatography. Gas chromatography−mass spectrometry (GC-MS) analyses were performed by means of an Agilent Technologies 7890A GC system equipped with a HP-5 capillary column (5% phenyl methyl siloxan, 30 m × 250 μm × 0.25 μm) interfaced with an Agilent 5975N MSD scheme operating in electron impact (EI) mode. The helium carrier gas flow rate was 14 mL/min, and the temperature was increased from 100 to 280 °C at a temperature ramp rate of 15 °C/min. The column was held at the initial and final temperatures for 5 min. Tetrabutylammonium perchlorate (Bu_4NClO_4, Sigma-Aldrich, >99%), used as supporting electrolyte, was recrystallized twice from 2-propanol. Milli-Q water (>18 MΩ cm) was used to prepare solutions, chemical reactions, and surface cleaning procedures. Dichloromethane, 2-propanol, and ethanol for surface cleaning procedures were redistilled prior to use. Prime-grade, single-side-polished silicon wafers (100-oriented (⟨100⟩ ± 0.5°), p-type (boron-doped), 500 ± 25 μm thick, with nominal resistivity of 0.001−0.003 Ω cm) were obtained from Siltronix, S.A.S. (Archamps, France) and are referred to as highly doped. Prime-grade, single-side-polished silicon wafers (100-oriented (⟨100⟩ ± 0.09°), n-type (phosphorus-doped), 500 ± 25 μm thick, 1−10 Ω cm resistivity) were purchased from Virginia Semiconductors, Inc. (Fredericksburg, VA) and are referred to as lowly doped.

2.2. Surface Modification. *2.2.1. Acetylene-Functionalized Silicon(100) Electrodes (S-1).* Assembly of the acetylenylated Si(100) surface (**S-1**) by covalent attachment of the diyne **1** followed a previously reported procedure (Scheme 1).[12] In brief, silicon wafers were cut into pieces (approximately 10 × 30 mm^2), cleaned for 20−30 min in hot Piranha solution (100 °C, a 3:1 (v/v) mixture of concentrated sulfuric acid to 30% hydrogen peroxide), rinsed with water and then etched with a deoxygenated 40% aqueous ammonium fluoride solution for 5 min. (***Caution:*** *Piranha solution is a strong oxidant and reacts violently with organic substances.*) The samples were then transferred, taking extra care to exclude air completely from the reaction vessel (a custom-made Schlenk flask), to a degassed (through a minimum of 30 min of argon bubbling) sample of diyne **1**. The samples were kept under a stream of argon while the reaction vessel was immersed in an oil bath set to 160 °C for 3 h. The flask was then opened to the atmosphere, and the functionalized surface samples (**S-1**) were rinsed several times with dichloromethane and rested for a 12 h period in a sealed vial at +4 °C under dichloromethane before being further reacted with the TEMPO molecule **2**.

2.2.2. CuAAC Attachment of 4-Azido TEMPO onto the Acetylenyl Surface (S-2). CuAAC reactions were used to attach 4-azido-TEMPO (**2**) to the acetylenyl surface (**S-1**). To a reaction vial containing the alkyne-functionalized silicon surface (**S-1**) was added (i) the azide (**2**, 0.5 mM, 2-propanol/water, 1:1), (ii) copper(II) sulfate pentahydrate (20 mol % relative to the azide), and (iii) sodium ascorbate (100 mol % relative to the azide). Reactions were carried out in air at room temperature under ambient light, and unless noted otherwise, they were stopped by removal of the samples from the reaction vessel after a reaction time of 2 h. The surface-bound [1,2,3]-triazoles (**S-2**) were

DOI: 10.1021/jacs.6b04788
J. Am. Chem. Soc. 2016, 138, 9611−9619

rinsed consecutively with copious amounts ethanol, water, ethanol, and dichloromethane and blown dry in argon before being analyzed.

2.3. Surface Characterization. *2.3.1. X-ray Photoelectron Spectroscopy.* X-ray photoelectron spectra (XPS) were obtained on an ESCALAB 220iXL spectrometer fitted with a monochromatic Al Kα source (1486.6 eV), a hemispherical analyzer and a 6 multichannel detector. Spectra of Si 2p (89−108 eV), C 1s (276−295 eV), N 1s (391−410 eV), and O 1s (523−542 eV) were recorded in normal emission (θ = 90°) with the analyzing chamber operating below 10^{-9} mbar. The resolution of the spectrometer is ca. 0.6 eV as measured from the Ag $3d_{5/2}$ signal (full width at half-maximum, fwhm) with 20 eV pass energy. High-resolution scans were run with 0.1 eV step size, dwell time of 100 ms, and the analyzer pass energy set to 20 eV. After background subtraction, spectra were fitted with Voigt functions. All energies are binding energies expressed in electronvolts, obtained by applying to all samples a rigid shift to bring the energy of the C 1s peak to a value of 285.0 eV.

2.3.2. X-ray Reflectometry. X-ray reflectivity (XRR) profiles of **S-2** samples (highly doped) were measured under ambient conditions on a Panalytical Ltd. X'Pert Pro Reflectometer using Cu Kα X-ray radiation (λ = 1.54056 Å). The X-ray beam was focused using a Göbel mirror and collimated with 0.2 mm presample slit and a postsample parallel plate collimator. Reflectivity data were collected over the angular range $0.05° \leq \theta \leq 5.00°$, with a step size of 0.010° and counting time of 10 s per step. Prior to measurements, samples were stored under argon and exposed to air for approximately 10 min in order to be aligned on the reflectometer. From the experimental data, structural parameters of the self-assembled structures were refined using the MOTOFIT analysis software with reflectivity data presented as a function of the momentum transfer vector normal to the surface $Q = 4\pi(\sin\theta)/\lambda$.[23] The Levenberg−Marquardt method was used to minimize χ^2 values in the fitting routines.

2.3.3. Electrochemical Characterization. Electrochemical experiments of the silicon electrodes (**S-2** samples) were performed in a PTFE three-electrode cell with the modified silicon surface as the working electrode, a platinum wire (ca. 30 mm^2) as the counter electrode, and a plastic body silver/silver chloride "leakless" as the reference electrode (eDAQ, part ET072−1). The reference electrode was checked against the ferrocene/ferricenium couple (Fc^+/Fc) at a glassy carbon electrode before and after each experiment. All potentials are reported versus the formal potential, E_f^0, for the Fc^+/Fc couple (1.0×10^{-3} M ferrocene solutions in acetonitrile containing either Bu_4NPF_6, Bu_4NClO_4, Bu_4NO_3, Bu_4HSO_4, or $Bu_4NCF_3SO_3$). All solutions for electrochemical measurements of contained 1.0×10^{-1} M of the Bu_4N salt as supporting electrolyte. The surface coverage, Γ, in mol cm^{-2}, was calculated from the faradaic charge taken as the background-subtracted integrated anodic current. All electrochemical experiments were performed at room temperature (23 ± 2 °C) in a grounded Faraday cage in air and either shielded from ambient light or deliberately illuminated (lowly doped samples, when stated) using a fiber-coupled high-power tungsten source from World Precision Instruments (model Novaflex optical illuminator) with a an output of approximately 4500 lx. A rectilinear cross-sectional Viton gasket defined the geometric area of the working electrode to 28 mm^2. The back side of the silicon sample was exposed with emery paper and rubbed with gallium−indium eutectic. A planar copper electrode was pressed against the sample backside and served as ohmic contact. Electrochemical measurements were performed using a CH instruments 650D electrochemical analyzer (CH Instruments, Inc.). The 95% confidence limit of the mean of experimentally determined quantities, such as surface coverage Γ, and the voltage of the current peaks are calculated as $t_{n-1}s/n^{1/2}$, where t_{n-1} depends on the number of repeats and varied between 3.18 and 2.23,[24] s is the standard deviation, and n is the number of repeated measurements (n was between 3 and 10). The device flat-band potential (E_{fb}) was estimated for **S-2** samples on lowly doped electrodes from measurements of the open-circuit voltage (OCP) under illumination (Figure S7).[25] Experimental cyclic voltammograms of **S-2** samples were analyzed by a commercial digital simulation program (DigiElch 7, ElchSoft). Butler−Volmer kinetics was used to estimate charge transfer parameters. A semi-infinite 1D diffusion at an electrode of planar geometry was assumed; all diffusion coefficients were set to 1×10^{-5} cm^2 s^{-1}. The number of equally spaced nodes in the spatial grid perpendicular to the electrode was set to 39. The adsorption process is simulated on the basis of the Frumkin isotherm using different values for the self-interaction parameter a. Simulations in DigiElch of the surface redox reaction require modeling a system made up by two redox couples, and charge-transfer is assumed to proceed only by direct reduction/oxidation of the adsorbed species. The first couple (*sln.*), does not undergo a charge-transfer reaction (k was set to 0.0 s^{-1}), and it is entered for the sole purpose of mimicking a species adsorbed on the electrode surface. The independent variables that describe the adsorption, i.e., the forward rate constant k_f and the equilibrium constant $K = k_f/k_b$ describing the adsorption process, were set to 1×10^{10} and 1×10^{14}, respectively. Observed electrocatalytic curves were compared against those of simulations for a system comprising two redox couples. One of these redox couples is the TEMPO unit strongly adsorbed on the electrode surface and plays the role of a redox mediator for the heterogeneous oxidation of bromide to bromine (written in DigiElch as $Br^- \rightarrow Br^\bullet + e^-$). The anodic wave does not plateau because this process is not the more common diffusive EC′ mechanism. The follow-up homogeneous chemical step for the formation of tribromide anion from bromide was not considered in the simulation.[26] The standard potential and rate constant of the adsorbed redox couple were set to the experimental values of **S-2** samples on either illuminated lowly doped or dark highly doped electrodes, $D_{Br-} = D_{Br\bullet} = 1 \times 10^{-5}$ cm^2 s^{-1}, the $Br^-/Br^\bullet$ electrochemical process was neglected (k_0 = 0 cm s^{-1}), and the speed (k_F) of the heterogeneous reaction occurring between the adsorbed and not adsorbed redox couple is varied (oxoammonium + $Br^- \xrightarrow{k_f}$ TEMPO + $Br^\bullet$).

2.4. Computational Methods. High-level *ab initio* calculations were used to predict the interaction energies between the Bu_4N counter-anions (HSO_4^-, NO_3^-, ClO_4^-, $CF_3SO_3^-$, and PF_6^-) and oxidized **S-2** film. For these calculations, we utilized a truncated model of the **S-2** film containing the (oxidized) TEMPO ring substituted with the 4-methyl-1,2,3-triazole substituent (denoted **T-cat** for short). Calculations were performed at a high level of theory, chosen on the basis of our previous studies of the redox behavior of nitroxide radicals.[27] We utilized the high-level composite *ab initio* G3-(MP2,CC)(+) method, a variation of standard G3(MP2,CC) theory[28] where calculations with the 6-31G(d) basis set are replaced with the 6-31+G(d) basis set (for better treatment of anions). This high-level methodology was utilized in conjugation with an ONIOM inspired approximation,[29] with RMP2/GTMP2Large employed to model remote substituent effects. All geometry optimizations and frequencies calculations were performed at the M06-2*X*/6-31+G(d,p) level of theory[30] and frequencies were scaled by recommended factors.[31] The SMD model was used to correct for implicit solvation effects.[32] All standard *ab initio* calculations were performed using the Gaussian 09[33] and Molpro 2012 software packages.[34]

To ensure maximum systematic error cancellation, we considered only the relative ΔG_{IP} values. These were converted to absolute values using the experimental redox potential for the HSO_4^- salt as the reference species. This approach is analogous the proton exchange method, which is able to provide accurate pK_a values even when absolute pK_a predictions (those that do not use a reference acid) are significantly less accurate.[35] The calculated absolute ΔG_{IP} values, along with the optimized geometries and all associated computational data and detailed theoretical procedures, are provided in the Supporting Information.

3. RESULTS AND DISCUSSIONS

The grafting of the TEMPO moieties (**S-2**, Scheme 1) onto the acetylene-terminated Si(100) surfaces (**S-1**) was initially verified by XRR and XPS. XRR allows the thickness (d) of thin films to be measured with atomic resolution as a result of the high contrast in scattering length density (SLD)[36] of the organic molecules in the SAM (SLD ≈ 1×10^{-5} $Å^{-2}$)

DOI: 10.1021/jacs.6b04788
J. Am. Chem. Soc. 2016, 138, 9611−9619

compared to those of air (SLD = 0) and the silicon substrate (SLD = 2.01 × 10^{-5} Å^{-2}). Figure 1 shows the measured

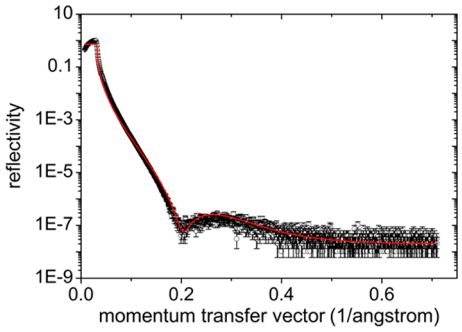

Figure 1. XRR profile of TEMPO monolayers (**S-2**) assembled on Si(100) electrodes by CuAAC reactions of 4-azido TEMPO on monolayers of 1,8-nonadiyne.

specular XRR curve for **S-2** samples. The theoretical fit to the experimental data is shown as a solid line.[23] Unlike the Fresnel-like decay of the Si(100)−H surface,[37] XRR profiles for **S-2** show clear interference thickness oscillations that could be simulated using a one-layer model of 16 Å thickness, which is close to the theoretical length of 14 Å. The refined value of scattering length density for the CuAAC-modified substrates (**S-2**) is 14.1 × 10^{-6} Å^{-2} and as high as those achieved for SAMs on gold substrates in close-packed Langmuir−Blodgett films.[38] The surface roughness between the silicon surface and the monolayer, as determined by XRR refinement, was 2.9 Å, which is typical for high-quality silicon substrates.[39] XPS spectra acquired for **S-2** samples are shown in Figure S1. This appearance of the N 1s electrons after the CuAAC reaction is in good agreement with the literature for analogous derivatization procedures on solid surfaces.[12b] There was no evidence for the high binding energy N 1s signal (ca. 405 eV)[40] that corresponds to the electron-deficient nitrogen atom in the azido group, hence confirming negligible physisorption of the radical species in the film. A least-squares refinement of the N 1 emission gives three fitted peaks with binding energies of 400.4, 401.7, and 402.7 eV. The position of the main low binding energy line in the **S-2** samples is in agreement with the 400.6 eV previously assigned to nitroxide nitrogen atoms in thin films of the *p*-nitrophenyl nitroxide radical.[41] Electrons from the triazole heterocycle contributed to the 400.4 and 401.7 emissions only, with an expected ratio of the peak areas being ca. 2:1.[12b,42] The weak shoulder observed on the high binding energy side (402.7 eV) is be tentatively assigned to a shakeup satellite[43] of N−O electrons.

Figure 2a shows cyclic voltamograms for **S-2** samples prepared on highly doped electrodes. The TEMPO films exhibited cyclic voltammetry waves of moderate stability (Figure S2) attributable to the chemically reversible nitroxide/oxoammonium ion oxidation/reduction process[15b] and with a surface coverage Γ = 2.21 ± 0.09 × 10^{-10} mol cm^{-2} and the magnitude of the peak scales with the voltage scan rate (ν) and not with the square root of ν, which is indicative of an electroactive substrate-bound monolayer (Figure S3). With only few exceptions,[44] for most electrochemical experiments, a large excess of an inert electrolyte salt is necessary. This is done to restrict the potential gradient only within a distance of few nanometers from the surface and to compensate for charges created upon electron transfer, hence preventing an increase in

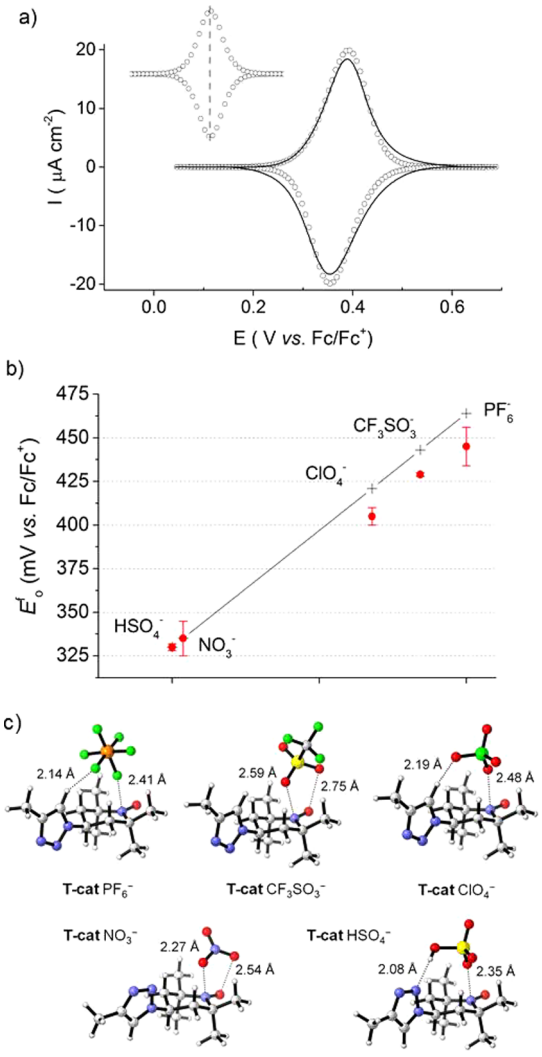

Figure 2. Cyclic voltammetry for **S-2** samples prepared on Si(100) electrodes (highly doped, 0.001−0.003 Ω cm). (a) Background-subtracted observed (solid line) and simulated (symbols) voltammograms at 100 mV s^{-1} in MeCN containing 1.0 × 10^{-1} M Bu_4NClO_4. Inset shows the simulated voltammetry for a reversible and noninteracting electroactive monolayer system (k was set to 10^4 s^{-1} and Frumkin "a" was set to zero). Ideal adsorptive-shaped waves are symmetric with respect to E_f^0 and show a 90.6/n fwhm. (b) Shifts of the experimental E_f^0 (red circles) and changes to the theoretical redox potential (+) as a function of the chemical composition of the electrolyte anion (Tables S1 and S2). (c) M06-2X/6-31+G(d,p) optimized geometries of the complexes between electrolyte anions and a truncated model of the **S-2** film containing the oxidized TEMPO substituted with the 4-methyl-1,2,3-triazole substituent (denoted **T-cat**).

local resistivity during the experiment. In a high dielectric constant solvent such as acetonitrile, the electrochemical behavior of self-assembled monolayers depends strongly on the nature of the supporting electrolytes,[45] and ion pairing with the redox unit is known to affect both kinetics and thermodynamics.[46]

Figures 2b and S4 display CV data of TEMPO monolayers in acetonitrile solutions containing different Bu_4N salts. Notably, the positions of the anodic and cathodic peaks appear to relate to the anion chemistry; the apparent formal potential (E_f^0) moves progressively anodically in the sequence HSO_4^- < NO_3^- < ClO_4^- < $CF_3SO_3^-$ < PF_6^- (Table S1). With the exception of

DOI: 10.1021/jacs.6b04788
J. Am. Chem. Soc. 2016, 138, 9611−9619

HSO_4^-, the magnitude of the displacement in E_f^0 tracks the empirical value of the anion Lewis basicity (Figure 2b and Table S2, *vide infra*). In the case of HSO_4^-, theoretical calculations (Tables S3−S5) indicate that the additional stabilization is due to formation of a hydrogen bond with azole ring (Figure 2c). The value of Γ was approximately 50% of that reported for close-packed TEMPO monolayers assembled on gold electrodes,[47] but even for this "diluted", system the shape of the experimental redox waves is not ideal,[15b] showing a minor asymmetry. The experimental fwhm is also independent of surface coverage in the range of Γ explored (Figure S5), yet is larger than the theoretical values of 90.6/n mV (Figure 2a inset). For instance, the observed fwhm is ca. 100 mV for ClO_4^-- or NO_3^--based electrolytes (102 ± 1 and 94 ± 6 mV, respectively) and upward to ca. 112 ± 1 and 119 ± 3 mV in $CF_3SO_3^-$ and PF_6^- solutions, respectively (Table S1). A small peak asymmetry coupled to a small increase (ca. 5−10 mV) over the ideal fwhm's can be simulated and accounted for in terms of slow charge transfer kinetics (Figure 2a, simulated CV in symbols with refined electrochemical rate constant k and refined fwhm being 3.6 s^{-1} and 96 mV, respectively). At present, we are unsure as to what factors other than slow kinetics contribute to the nonideal fwhm's in the ClO_4^- and PF_6^- systems especially because these nonidealities persist when the rate is enhanced by up to 5-fold for illuminated lowly doped substrates (*vide infra*).

We note, however, that a large number of models have been proposed to explain such nonidealities,[48] and in the Nernstian case of an electrochemically reversible system ($k \rightarrow \infty$),[49] when the energy of interaction between like molecules is larger than that between unlike molecules, the observed fwhm will be larger than that for the ideal noninteracting case.

In reversible systems, the extent of these putative electrostatic interactions have often been parametrized simply by introducing changes to the Frumkin a factor that leads to the corresponding isotherm (Figure S6).[50] However as noted above, our highly doped **S-2** systems have finite electron transfer kinetics; hence, using this approach would probably lead to an oversimplification and would fail to give a meaningful quantitative explanation on both peak broadening and shifts in E_f^0 values. In our discussion we therefore focus exclusively on the electrolyte-related shifts to E_f^0 and interpret the data by showing a correlation between the observed voltammograms and calculated quantities. Notably, the displacement in E_f^0 (Table S2) tracks the empirical value of the anion Lewis basicity with the exception of HSO_4^- for which, as noted above, a favorable hydrogen bond with the azole ring leads to additional stabilization. An electrostatic component can be separated for the Lewis acid−base interaction (oxoammonium−electrolyte anion interaction), and this electrostatic scheme brings about a reduction in the thermodynamic cost for the TEMPO oxidation. This is supported by the theoretical calculations of the oxoammonium−electrolyte anion interaction energies that are stabilizing overall (see Supporting Information) and predict a progressive anodic shift in the redox potential in the same order as in experiment: $HSO_4^- < NO_3^- < ClO_4^- < CF_3SO_3^- < PF_6^-$. In brief, the nature of the electrolyte anion appears to have a large effect on i−E curves in a way that is not quantifiable as a commonly reported adjustment of the Frumkin a term (Figure S6). The direction of the displacement in E_f^0 values is consistent with the chemistry involved, and this implies that for a given bias one is able to predictably alter the ratio of surface reductant to surface oxidant, i.e., surface nitroxide to oxoammonium, by a simple change in the electrolyte; for instance, increasing the oxidizing power of a TEMPO film by increasing the Lewis base character of the electrolyte anion. This aspect is potentially of great significance when one considers applications of TEMPO films in heterogeneous catalysis.[51] To illustrate this, we have coupled the homogeneous TEMPO charge transfer reaction to the heterogeneous oxidation of bromide ions and extracted the dependency of the apparent heterogeneous rate constant as a function of electrolyte, with the highest k_{cat} measured for PF_6^- systems (Figure S8).

As introduced above, our chemical strategy to immobilize the nitroxide radical on the highly doped substrate can be expanded to a Si(100) electrode of low doping where the internal electrical field of the semi conductor space-charge[52] can be used to drive the redox reaction(s) contrathermodynamically (Figure 3). The same surface chemistry used for the **S-2** samples on the

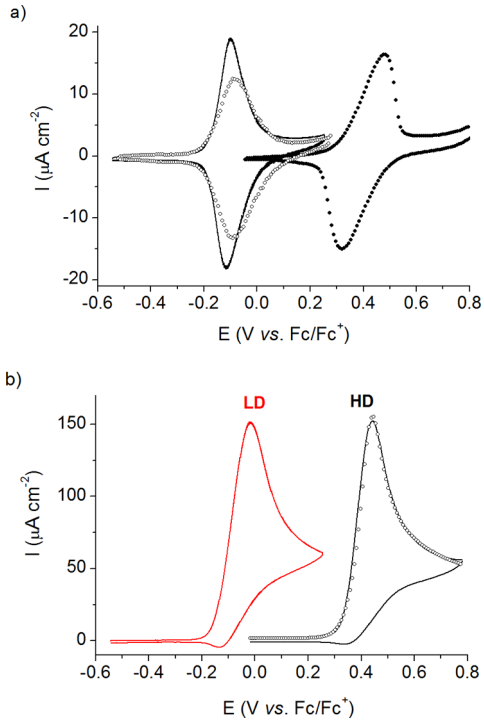

Figure 3. Cyclic voltammograms for **S-2** samples prepared on n-Si electrodes (lowly doped, 1−10 Ω cm). (a) Dark oxidation and reduction waves (symbols) and their underpotential shift with supra band gap illumination (lines). CVs were obtained at a voltage sweep rate of 100 mV s^{-1} in MeCN containing 1.0 × 10^{-1} M of either Bu_4NClO_4 (solid line, fwhm = 91 mV) or Bu_4NPF_6 (empty symbols, fwhm =120 mV). (b) Observed (lines) and simulated (symbols) CV of the electrocatalytic mechanism on illuminated lowly or highly doped **S-2** samples (LD or HD, respectively) in the presence of 0.5 × 10^{-3} M Bu_4NBr in 1.0 × 10^{-1} M of Bu_4NPF_6. The refined value of k_{cat} for the reaction between the adsorbed oxoammonium and nonadsorbed bromide was 3.2 × 10^3 M^{-1} s^{-1}.

highly doped electrodes (Figure 2) was applied to n-type Si(100) electrodes of low doping (ND, ∼4.5 × 10^{14} to 5.0 × 10^{15} cm^{-3}, resistivity = 1−10 Ω cm). The dark current−voltage characteristics of the **S-2** electrode (Figure 3a, symbols) reveal the extent of the expected kinetic limitations for the tunneling across the semiconductor space-charge; both asymmetry in the peaks[53] and a sizable peak-to-peak separation are a manifestation of slow charge transfer kinetics (k_{et} ≈ 0.01 s^{-1}) in the

DOI: 10.1021/jacs.6b04788
J. Am. Chem. Soc. 2016, 138, 9611−9619

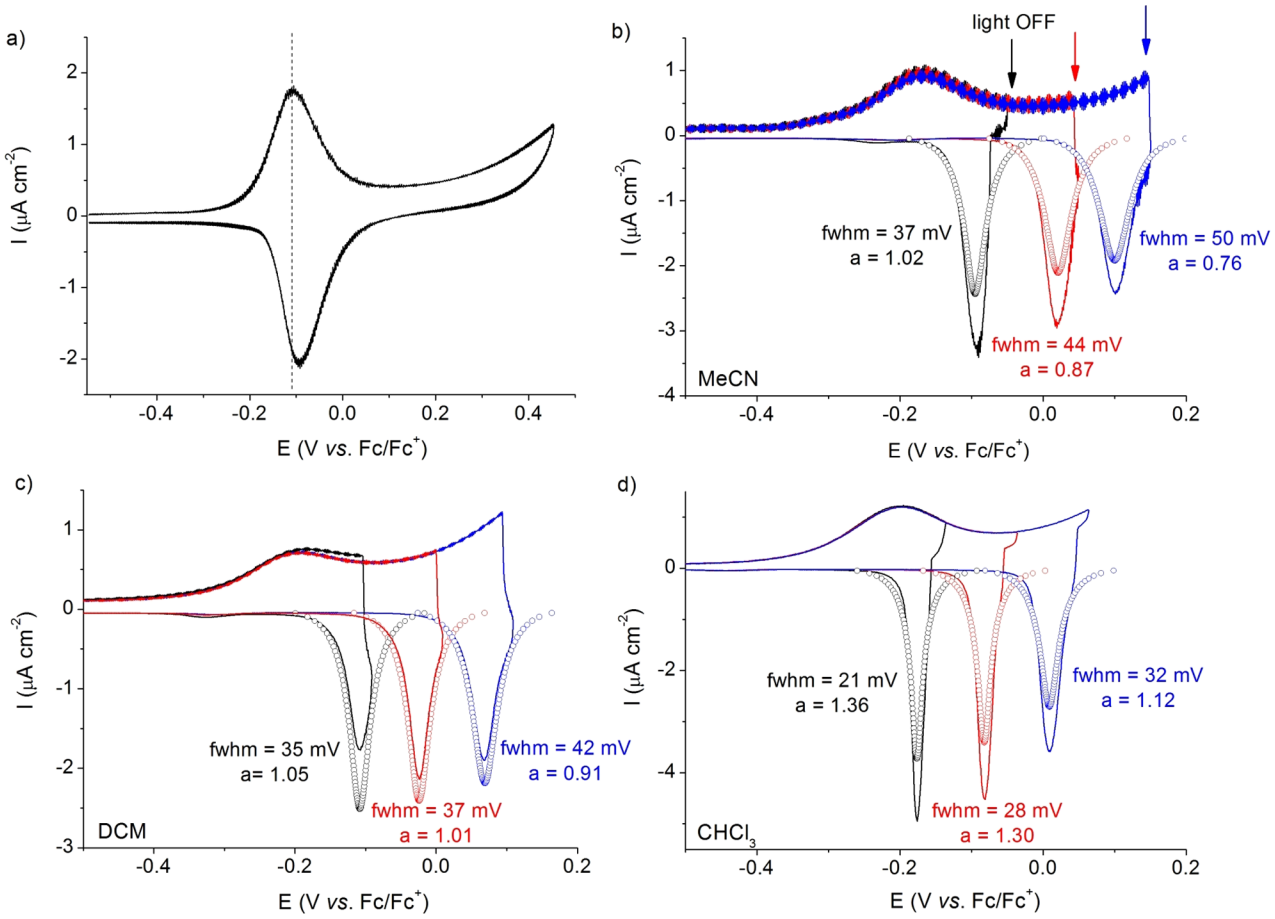

Figure 4. (a) Example of "peak inversion" in CVs of **S-2** electrodes of low doping under illumination (Bu_4NClO_4 and ν = 100 mV s^{-1}). (b–d) "Peak inversion" can be deliberately induced in CVs of **S-2** samples on lowly doped electrodes when illumination is switched off at the anodic vertex (0.4, 0.5, or 0.6 V) in Bu_4NClO_4 electrolytes using solvents of progressively lower dielectric constant (37.5 for acetonitrile, 8.9 for dichloromethane, and 4.8 for chloroform). Simulated voltammograms (symbols) and refined values of the self-interaction parameter "*a*" are indicated in figure.

dark lowly doped samples. In the light-activated faradaic response,[8,54] this kinetic barrier is largely removed (Figure 3a, solid line, $k_{et} \approx 15$ s^{-1}), and the values of E_f^0 are shifted approximately 500 mV more negative with respect to the low or high doping **S-2** samples in the dark (Figure 2a). Peak shapes in the illuminated lowly doped samples are near-to-ideal (fwhm = 95 ± 7 mV) in ClO_4^- electrolytes but remain significantly broader in PF_6^- (fwhm = 131 ± 5 mV), hence reinforcing the notion that factors other than kinetics are causing this nonideality (*vide supra*). The uphill shift is consistent with the measured OCP under illumination (Figure S7a) and is a result of a process mediated by photogenerated valence band holes as previously reported for gallium and germanium photoanodes.[52,55] As anticipated in the introduction, the shift in the E_f^0 of the homogeneous TEMPO reaction can translate into an energetic gain for a heterogeneous reaction, such as the oxidation of bromide ions in solution. The electrocatalytic process that is mediated by the surface TEMPO molecule on illuminated lowly doped samples (Figure 3b) is shifted uphill by about 500 mV compared to the same heterogeneous reaction on highly doped (metallic) samples (Figure S8).

The CV data for illuminated **S-2** samples of low doping have been reproduced several times, with no major differences in peak-to-peak separations (11.5 ± 1.5 mV), fwhm (95 ± 7 mV), and Γ (2.05 ± 0.04 × 10^{-10} mol cm^{-1}) values (ClO_4^- data); however, a remarkable phenomenon was observed in at least four independently prepared and analyzed samples (Figures 4a and S7). In these four samples, the cathodic current peaked at a more anodic potential than that of the anodic peak. A current across an electrified interface is always indicative of an overall rate; hence, this "inversion" would immediately be disregarded as an artifact on a common metallic surface. However, a similar observation was reported in 1979 by Wrighton and co-workers for illuminated n-type gallium arsenide electrodes[52] that were modified with surface-bound ferrocenes. As tentatively suggested by Wrighton, a reduction rate being higher than the oxidation rate at an anodic regime may result from the charges of the adsorbed oxidized species affecting the electrostatics of the semiconductor electrode.[56] In the cases at hand (**S-2**, n-type, low doping), the flat-band potential of the system, E_{fb}, may be forced to shift anodically when during the voltammetric sweep the relative amount of neutral nitroxide radical to positively charged oxoammonium ion changes in favor of the latter. The observed sudden dominance of the reduction rate at a bias that is anodic of the oxidation wave may result from an electrostatic effect on the semiconductor space-charge, such that the oxoammonium species force bands to flatten, removing the tunneling barrier for the electrons leaving the electrode. It is important to note that the light intensity used in our experiments appears not to be high enough to force the bands to flatten completely (Figure S7a) and that the high dielectric medium (ε_{MeCN} = 37.5) is not completely masking

DOI: 10.1021/jacs.6b04788
J. Am. Chem. Soc. 2016, 138, 9611–9619

interactions between the ionized semiconductor space-charge and oxoammonium species. Because of this electrostatic "push" by the oxoammonium species on the space-charge, the onset of depletion requires a more positive bias, hence resulting in an oxoammonium-assisted smaller barrier to the flow of cathodic currents across the interface.

To support this electrostatic explanation for the "peak inversion" phenomenon, we performed voltammetry in solvents of different dielectric constants to minimize or amplify this putative electrostatic effect, and we deliberately switched off the illumination source precisely at the anodic vertex. Figure 4b–d shows a series of CVs for **S-2** samples on lowly doped electrodes, with only the sweep toward the anodic region performed under illumination. The anodic "illuminated" wave in Figure 4 has nothing unusual; hence, the theoretical current–voltage characteristics can be simulated on the basis of the Frumkin isotherm using a "zero" value of the Laviron self-interaction parameters *a*, i.e., the Langmuir isotherm without interactions[57] involving TEMPO units (*vide infra*). From a different angle, the observed peak shape implies ideality in the sense that the surface concentrations of the reduced and oxidized species equal their activities.[53] The light is then switched off at the anodic vertex (set either as 0.4, 0.5, or 0.6 V) in order to deliberately introduce a space-charge barrier for electrons to enter the semiconductor (anodic reaction). The flux of photogenerated holes is brought to a sudden halt, and a very sharp reductive peak appears instantly. The net result is a sudden increase in the reduction rate when the light is switched off, i.e., under these conditions the reductive peaks occur at a potential that is more positive than the oxidative peak. By doing this, we have supported the above hypothesis of the "peak inversion" (Figure 4a) being the result of an electrostatic effect of the oxoammonium on the semiconductor space-charge. Furthermore, we can now assume that the reduction event is fast and behaves similar to a Nernstian process; hence, we can tentatively analyze our adsorbed system by using models that hold for reversible systems. As introduced above, a conventional approach to quantify the observed drop in experimental fwhm's in terms of attractive forces is the parametrization developed by Laviron based on the Frumkin isotherm (Figures 4, S6, and S9 and section §S1). In this model, the voltammetry response is derived under Nernstian conditions by taking into account a simple isotherm, the so-called Frumkin isotherm, which introduces the *a* parameter. This is a dimensionless constant describing the extent of attractive and repulsive interactions between molecules,[58] and is directly related to the fwhm value (Supporting Information section §S1). When the light source is switched off at the anodic vertex, band-bending in the depleted semiconductor space-charge is rapidly restored, and the balance of attractive to repulsive forces experienced by the adsorbed oxoammonium species appears to tilt in favor of the attractions, with the refined *a* increasing above the zero value (Figure 4b–d). In line with this explanation, this putative electrostatic effect on the *a* self-interaction parameter, which we ascribe tentatively to a space-charge effect on the oxoammonium/anion attractions, becomes in fact more pronounced as the solvent dielectric is reduced by moving from acetonitrile to chloroform solutions (Figure 4b,d).

4. CONCLUSIONS

This article presented a two-step acetylenylation/click procedure as a wet chemistry approach to tether a nitroxide radical to a silicon surface and preserve its open-shell state. This is the first example of the attachment of a redox-active stable free radical onto a semiconducting surface. From a fundamental standpoint, these surface systems can be used as a laboratory model to explore the recently reported electrostatic effects on chemical bonding and reactivity.[3,59] Here we have explored to what extent electrostatic effects arising either from electrolyte species or ionized dopants in the semiconductor space-charge can influence the redox activity of the free radical. We have shown experimentally that it is possible to gauge these effects as changes to voltammetric responses. This knowledge may aid the development of electrocatalytic heterogeneous systems where the redox reaction of interest can be coupled to semiconductor effects and therefore driven contra-thermodynamically by up to 0.5 V.

All experimental results show good agreement with theoretical calculations and show that the redox properties of nitroxide radical monolayer can indeed be predictably manipulated by controlling the electrostatics between the tethered persistent radical and electrolytes or semiconductor.

■ ASSOCIATED CONTENT

Supporting Information

The Supporting Information is available free of charge on the ACS Publications website at DOI: 10.1021/jacs.6b04788.

Synthetic methods, XPS data, additional theoretical data, geometries and procedures, additional electrochemical data and simulations (PDF)

■ AUTHOR INFORMATION

Corresponding Authors

*gwallace@uow.edu.au
*michelle.coote@anu.edu.au
*sciampi@uow.edu.au

Present Address

S.C., N.D.: Department of Chemistry, Curtin University, Bentley WA 6102, Australia.

Notes

The authors declare no competing financial interest.

■ ACKNOWLEDGMENTS

L.Z. thanks University of Wollongong and the for scholarship support. S.C. thanks the University of Wollongong for the Vice Chancellor Fellowship. Support from the Australian National Fabrication Facility (ANFF) Australian Institute of Nuclear Science and Engineering is acknowledged. V.R.G. thanks CAPES-Brazil (Proc. 12149-13-6) for the conceded scholarship. G.G.W., M.L.C., J.J.G., and S.C. gratefully acknowledge financial support from the Australian Research Council under their Centre of Excellence and Discovery Project Schemes (CE140100012, DP150103065) and generous allocations of supercomputing time on the National Facility of Australian National Computational Infrastructure is acknowledged.

■ REFERENCES

(1) (a) Gooding, J. J.; Ciampi, S. *Chem. Soc. Rev.* **2011**, *40*, 2704–2718. (b) Chia, S.; Cao, J.; Stoddart, J. F.; Zink, J. I. *Angew. Chem., Int. Ed.* **2001**, *40*, 2447–2451.

(2) Fischer, H. *Chem. Rev.* **2001**, *101*, 3581–3610.

(3) (a) Klinska, M.; Smith, L. M.; Gryn'ova, G.; Banwell, M. G.; Coote, M. L. *Chem. Sci.* **2015**, *6*, 5623–5627. (b) Gryn'ova, G.; Marshall, D. L.; Blanksby, S. J.; Coote, M. L. *Nat. Chem.* **2013**, *5*, 474–

DOI: 10.1021/jacs.6b04788
J. Am. Chem. Soc. 2016, 138, 9611–9619

481. (c) Gryn'ova, G.; Coote, M. L. *J. Am. Chem. Soc.* **2013**, *135*, 15392−15403.
(4) Knoop, C. A.; Studer, A. *J. Am. Chem. Soc.* **2003**, *125*, 16327−16333.
(5) Niermann, N.; Degefa, T. H.; Walder, L.; Zielke, V.; Steinhoff, H.-J.; Onsgaard, J.; Speller, S. *Phys. Rev. B: Condens. Matter Mater. Phys.* **2006**, *74*, 235424.
(6) (a) Lloveras, V.; Badetti, E.; Chechik, V.; Vidal-Gancedo, J. *J. Phys. Chem. C* **2014**, *118*, 21622−21629. (b) Blinco, J. P.; Chalmers, B. A.; Chou, A.; Fairfull-Smith, K. E.; Bottle, S. E. *Chem. Sci.* **2013**, *4*, 3411−3415. (c) Swiech, O.; Bilewicz, R.; Megiel, E. *RSC Adv.* **2013**, *3*, 5979−5986.
(7) (a) Ball, P. *Nat. Mater.* **2005**, *4*, 119−119. (b) Ciampi, S.; Harper, J. B.; Gooding, J. J. *Chem. Soc. Rev.* **2010**, *39*, 2158−2183.
(8) Choudhury, M. H.; Ciampi, S.; Yang, Y.; Tavallaie, R.; Zhu, Y.; Zarei, L.; Gonçales, V. R.; Gooding, J. J. *Chem. Sci.* **2015**, *6*, 6769−6776.
(9) Jansen, R. *Nat. Mater.* **2012**, *11*, 400−408.
(10) Nakamura, M.; Yoshida, S.; Katayama, T.; Taninaka, A.; Mera, Y.; Okada, S.; Takeuchi, O.; Shigekawa, H. *Nat. Commun.* **2015**, *6*, 8465.
(11) Greene, M. E.; Guisinger, N. P.; Basu, R.; Baluch, A. S.; Hersam, M. C. *Surf. Sci.* **2004**, *559*, 16−28.
(12) (a) Ciampi, S.; Eggers, P. K.; Le Saux, G.; James, M.; Harper, J. B.; Gooding, J. J. *Langmuir* **2009**, *25*, 2530−2539. (b) Ciampi, S.; Böcking, T.; Kilian, K. A.; James, M.; Harper, J. B.; Gooding, J. J. *Langmuir* **2007**, *23*, 9320−9329.
(13) Squires, T. M.; Messinger, R. J.; Manalis, S. R. *Nat. Biotechnol.* **2008**, *26*, 417−426.
(14) Hartstein, A.; Kirtley, J. R.; Tsang, J. C. *Phys. Rev. Lett.* **1980**, *45*, 201−204.
(15) (a) Zanetti-Polzi, L.; Daidone, I.; Bortolotti, C. A.; Corni, S. *J. Am. Chem. Soc.* **2014**, *136*, 12929−12937. (b) Alévêque, O.; Blanchard, P.-Y.; Breton, T.; Dias, M.; Gautier, C.; Levillain, E.; Seladji, F. *Electrochem. Commun.* **2009**, *11*, 1776−1780. (c) Kwon, Y.; Mrksich, M. *J. Am. Chem. Soc.* **2002**, *124*, 806−812.
(16) Ng, A.; Ciampi, S.; James, M.; Harper, J. B.; Gooding, J. J. *Langmuir* **2009**, *25*, 13934−13941.
(17) Rohde, R. D.; Agnew, H. D.; Yeo, W.-S.; Bailey, R. C.; Heath, J. R. *J. Am. Chem. Soc.* **2006**, *128*, 9518−9525.
(18) (a) Coletti, C.; Marrone, A.; Giorgi, G.; Sgamellotti, A.; Cerofolini, G.; Re, N. *Langmuir* **2006**, *22*, 9949−9956. (b) Kondo, M.; Mates, T. E.; Fischer, D. A.; Wudl, F.; Kramer, E. J. *Langmuir* **2010**, *26*, 17000−17012.
(19) (a) Ubara, H.; Imura, T.; Hiraki, A. *Solid State Commun.* **1984**, *50*, 673−675. (b) Chabal, Y. J.; Higashi, G. S.; Raghavachari, K.; Burrows, V. A. *J. Vac. Sci. Technol., A* **1989**, *7*, 2104−2109. (c) Niwano, M.; Takeda, Y.; Ishibashi, Y.; Kurita, K.; Miyamoto, N. *J. Appl. Phys.* **1992**, *71*, 5646−5649.
(20) Nemanick, E. J.; Hurley, P. T.; Webb, L. J.; Knapp, D. W.; Michalak, D. J.; Brunschwig, B. S.; Lewis, N. S. *J. Phys. Chem. B* **2006**, *110*, 14770−14778.
(21) Meldal, M.; Tornøe, C. W. *Chem. Rev.* **2008**, *108*, 2952−3015.
(22) Tansakul, C.; Lilie, E.; Walter, E. D.; Rivera, F.; Wolcott, A.; Zhang, J. Z.; Millhauser, G. L.; Braslau, R. *J. Phys. Chem. C* **2010**, *114*, 7793−7805.
(23) Nelson, A. *J. Appl. Crystallogr.* **2006**, *39*, 273−276.
(24) Miller, J. N.; Miller, J. C. *Statistics and Chemometrics for Analytical Chemistry*, 6th ed.; Prentice Hall: Essex, U.K., 2010; p 266.
(25) Gerischer, H. *J. Electroanal. Chem. Interfacial Electrochem.* **1975**, *58*, 263−274.
(26) Allen, G. D.; Buzzeo, M. C.; Villagrán, C.; Hardacre, C.; Compton, R. G. *J. Electroanal. Chem.* **2005**, *575*, 311−320.
(27) (a) Gryn'ova, G.; Barakat, J. M.; Blinco, J. P.; Bottle, S. E.; Coote, M. L. *Chem. - Eur. J.* **2012**, *18*, 7582−7593. (b) Blinco, J. P.; Hodgson, J. L.; Morrow, B. J.; Walker, J. R.; Will, G. D.; Coote, M. L.; Bottle, S. E. *J. Org. Chem.* **2008**, *73*, 6763−6771. (c) Hodgson, J. L.; Namazian, M.; Bottle, S. E.; Coote, M. L. *J. Phys. Chem. A* **2007**, *111*, 13595−13605.
(28) Curtiss, L. A.; Raghavachari, K.; Redfern, P. C.; Baboul, A. G.; Pople, J. A. *Chem. Phys. Lett.* **1999**, *314*, 101−107.
(29) (a) Izgorodina, E. I.; Brittain, D. R. B.; Hodgson, J. L.; Krenske, E. H.; Lin, C. Y.; Namazian, M.; Coote, M. L. *J. Phys. Chem. A* **2007**, *111*, 10754−10768. (b) Coote, M. L.; Krenske, E. H.; Izgorodina, E. I. *Macromol. Rapid Commun.* **2006**, *27*, 473−497.
(30) Zhao, Y.; Truhlar, D. G. *Theor. Chem. Acc.* **2008**, *120*, 215−241.
(31) Alecu, I. M.; Zheng, J.; Zhao, Y.; Truhlar, D. G. *J. Chem. Theory Comput.* **2010**, *6*, 2872−2887.
(32) Marenich, A. V.; Cramer, C. J.; Truhlar, D. G. *J. Phys. Chem. B* **2009**, *113*, 6378−6396.
(33) Frisch, M. J.; Trucks, G. W.; Schlegel, H. B.; Scuseria, G. E.; Robb, M. A.; Cheeseman, J. R.; Scalmani, G.; Barone, V.; Mennucci, B.; Petersson, G. A.; Nakatsuji, H.; Caricato, M.; Li, X.; Hratchian, H. P.; Izmaylov, A. F.; Bloino, J.; Zheng, G.; Sonnenberg, J. L.; Hada, M.; Ehara, M.; Toyota, K.; Fukuda, R.; Hasegawa, J.; Ishida, M.; Nakajima, T.; Honda, Y.; Kitao, O.; Nakai, H.; Vreven, T.; Montgomery, J. A., Jr.; Peralta, J. E.; Ogliaro, F.; Bearpark, M.; Heyd, J. J.; Brothers, E.; Kudin, K. N.; Staroverov, V. N.; Kobayashi, R.; Normand, J.; Raghavachari, K.; Rendell, A.; Burant, J. C.; Iyengar, S. S.; Tomasi, J.; Cossi, M.; Rega, N.; Millam, J. M.; Klene, M.; Knox, J. E.; Cross, J. B.; Bakken, V.; Adamo, C.; Jaramillo, J.; Gomperts, R.; Stratmann, R. E.; Yazyev, O.; Austin, A. J.; Cammi, R.; Pomelli, C.; Ochterski, J. W.; Martin, R. L.; Morokuma, K.; Zakrzewski, V. G.; Voth, G. A.; Salvador, P.; Dannenberg, J. J.; Dapprich, S.; Daniels, A. D.; Farkas, O.; Foresman, J. B.; Ortiz, J. V.; Cioslowski, J.; Fox, D. J. *Gaussian 09*, revision E.01; Gaussian, Inc.: Wallingford, CT, 2009.
(34) (a) Werner, H.-J.; Knowles, P. J.; Knizia, G.; Manby, F. R.; Schütz, M.; Celani, P.; Korona, T.; Lindh, R.; Mitrushenkov, A.; Rauhut, G.; et al. *MOLPRO, a package of ab initio programs*, version 2012.1; University College Cardiff Consultants Limited: Cardiff, U.K., 2012. http://www.molpro.net. (b) Werner, H.-J.; Knowles, P. J.; Knizia, G.; Manby, F. R.; Schütz, M. *WIREs Comput. Mol. Sci.* **2012**, *2*, 242−253.
(35) Ho, J.; Coote, M. L. *Theor. Chem. Acc.* **2010**, *125*, 3−21.
(36) SLD for X-rays is obtained by multiplying the electron density ($e^-/Å^3$) of the material by the factor 2.82×10^{-5} Å.
(37) Ciampi, S.; James, M.; Darwish, N.; Luais, E.; Guan, B.; Harper, J. B.; Gooding, J. J. *Phys. Chem. Chem. Phys.* **2011**, *13*, 15624−15632.
(38) Ulman, A. *An Introduction to Ultrathin Organic Films: From Langmuir-Blodgett to Self-Assembly*; Academic Press Limited: London, U.K., 1991.
(39) (a) Linford, M. R.; Fenter, P.; Eisenberger, P. M.; Chidsey, C. E. D. *J. Am. Chem. Soc.* **1995**, *117*, 3145−3155. (b) Böcking, T.; James, M.; Coster, H. G. L.; Chilcott, T. C.; Barrow, K. D. *Langmuir* **2004**, *20*, 9227−9235. (c) James, M.; Darwish, T. A.; Ciampi, S.; Sylvester, S. O.; Zhang, Z.; Ng, A.; Gooding, J. J.; Hanley, T. L. *Soft Matter* **2010**, *7*, 5309.
(40) (a) Ciampi, S.; James, M.; Michaels, P.; Gooding, J. J. *Langmuir* **2011**, *27*, 6940−6949. (b) Devadoss, A.; Chidsey, C. E. D. *J. Am. Chem. Soc.* **2007**, *129*, 5370−5371.
(41) Caro, J.; Fraxedas, J.; Jürgens, O.; Santiso, J.; Rovira, C.; Veciana, J.; Figueras, A. *Adv. Mater.* **1998**, *10*, 608−610.
(42) (a) Liu, H.; Duclairoir, F.; Fleury, B.; Dubois, L.; Chenavier, Y.; Marchon, J.-C. *Dalton Trans.* **2009**, 3793−3799. (b) Qin, G.; Santos, C.; Zhang, W.; Li, Y.; Kumar, A.; Erasquin, U. J.; Liu, K.; Muradov, P.; Trautner, B. W.; Cai, C. *J. Am. Chem. Soc.* **2010**, *132*, 16432−16441.
(43) (a) Fraxedas, J.; Caro, J.; Figueras, A.; Gorostiza, P.; Sanz, F. *J. Vac. Sci. Technol., A* **1998**, *16*, 2517−2523. (b) Grobman, W. D.; Pollak, R. A.; Eastman, D. E.; Maas, E. T.; Scott, B. A. *Phys. Rev. Lett.* **1974**, *32*, 534−537.
(44) Compton, R. G.; Laborda, E.; Ward, C. R. *Understanding Voltammetry: Simulation of Electrode Processes*; Imperial College Press: London, U.K., 2014; p 145.
(45) (a) Gautier, C.; Alévêque, O.; Seladji, F.; Dias, M.; Breton, T.; Levillain, E. *Electrochem. Commun.* **2010**, *12*, 79−82. (b) Valincius, G.; Niaura, G.; Kazakeviciene, B.; Talaikyte, Z.; Kazemekaite, M.; Butkus, E.; Razumas, V. *Langmuir* **2004**, *20*, 6631−6638.

DOI: 10.1021/jacs.6b04788
J. Am. Chem. Soc. 2016, 138, 9611−9619

(46) Andreu, R.; Calvente, J. J.; Fawcett, W. R.; Molero, M. *J. Phys. Chem. B* **1997**, *101*, 2884−2894.
(47) Blanchard, P.-Y.; Alévêque, O.; Breton, T.; Levillain, E. *Langmuir* **2012**, *28*, 13741−13745.
(48) Honeychurch, M. J.; Rechnitz, G. A. *Electroanalysis* **1998**, *10*, 285−293.
(49) Laviron, E. *J. Electroanal. Chem. Interfacial Electrochem.* **1979**, *100*, 263−270.
(50) Forces betweeen like species are parametrized as a_A or a_B, whereas those between unlike species are indicated as a_{AB}. The peak shape relates to a, with a = $a_A + a_B - 2a_{AB}$. An *a* value > 0 is used for attractions, and a value < 0 is used for repulsions. For large values of *a*, the forward and backward peaks appear at different potential, regardless of kinetics.
(51) Kashiwagi, Y.; Uchiyama, K.; Kurashima, F.; Anzai, J.-i.; Osa, T. *Anal. Sci.* **1999**, *15*, 907−909.
(52) Bolts, J. M.; Wrighton, M. S. *J. Am. Chem. Soc.* **1979**, *101*, 6179−6184.
(53) Brown, A. P.; Anson, F. C. *Anal. Chem.* **1977**, *49*, 1589−1595.
(54) Yang, Y.; Ciampi, S.; Choudhury, M. H.; Gooding, J. J. *J. Phys. Chem. C* **2016**, *120*, 2874−2882.
(55) Bolts, J. M.; Wrighton, M. S. *J. Am. Chem. Soc.* **1978**, *100*, 5257−5262.
(56) Ginley, D.; Butler, M. *J. Electrochem. Soc.* **1978**, *125*, 1968−1974.
(57) Compton, R. G.; Banks, E. C. *Understanding Voltammetry*; Imperial College Press: London, U.K., 2011; p 282.
(58) Laviron, E. *J. Electroanal. Chem. Interfacial Electrochem.* **1974**, *52*, 395−402.
(59) Aragonès, A. C.; Haworth, N. L.; Darwish, N.; Ciampi, S.; Bloomfield, N. J.; Wallace, G. G.; Diez-Perez, I.; Coote, M. L. *Nature* **2016**, *531*, 88−91.

DOI: 10.1021/jacs.6b04788
J. Am. Chem. Soc. 2016, 138, 9611−9619